



CrossMark  
click for updates

Cite this: *RSC Adv.*, 2016, 6, 35152

# NaGd(WO<sub>4</sub>)<sub>2</sub>:Yb<sup>3+</sup>/Er<sup>3+</sup> phosphors: hydrothermal synthesis, optical spectroscopy and green upconverted temperature sensing behavior

Jinsheng Liao,\* Liling Nie, Qi Wang, Suijun Liu, He-Rui Wen and Jingping Wu

NaGd(WO<sub>4</sub>)<sub>2</sub>:Yb<sup>3+</sup>/Er<sup>3+</sup> (NGW:Yb<sup>3+</sup>/Er<sup>3+</sup>) phosphors co-doped with Yb<sup>3+</sup> (12–24 at%, at% *i.e.* atomic percent) and Er<sup>3+</sup> ions (1–10 at%) were synthesized by a facile hydrothermal process. Under 980 nm excitation, NGW:Yb<sup>3+</sup>/Er<sup>3+</sup> phosphors exhibited strong green upconversion (UC) emission bands centered at 532 nm (<sup>2</sup>H<sub>11/2</sub> → <sup>4</sup>I<sub>15/2</sub>) and 554 nm (<sup>4</sup>S<sub>3/2</sub> → <sup>4</sup>I<sub>15/2</sub>) and weak red emissions near 658 and 671 nm (<sup>4</sup>F<sub>9/2</sub> → <sup>4</sup>I<sub>15/2</sub>). The optimum doping concentrations of Er<sup>3+</sup> and Yb<sup>3+</sup> for the highest emission intensity were determined by using X-ray diffraction (XRD) and photoluminescence (PL) analyses. Concentration dependent studies revealed that the optimal composition was realized for the 20 at% Yb<sup>3+</sup> and 6.0 at% Er<sup>3+</sup>-doping concentration with a strong green emission. A possible UC mechanism for NGW:Yb<sup>3+</sup>/Er<sup>3+</sup> depends on the pump power is discussed. The temperature dependence of the fluorescence intensity ratios (FIR) for the two green UC emission bands peaking at 532 and 554 nm was studied in the range of 293–573 K under excitation by a 980 diode laser and the maximum sensitivity was approximately 114.96 × 10<sup>-4</sup> K<sup>-1</sup> at 453 K. This indicates that NGW:Yb<sup>3+</sup>/Er<sup>3+</sup> phosphors are potential candidates for optical temperature sensors with high sensitivity.

Received 15th January 2016

Accepted 21st March 2016

DOI: 10.1039/c6ra01283c

www.rsc.org/advances

## Introduction

Rare-earth (RE) ion doped upconversion (UC) materials have been widely investigated because of their broad application prospects in three-dimensional displays,<sup>1</sup> laser and optical amplifiers,<sup>2</sup> optical temperature sensors,<sup>3</sup> solar cells,<sup>4</sup> optical data storage<sup>5</sup> and bio-technologies.<sup>6,7</sup> Recently, applying these materials as temperature sensing media has attracted great attention.<sup>8–10</sup> In this application, optical temperature sensors based on the fluorescence intensity ratio (FIR) technique as a noninvasive thermometry are considered to be an alternative candidate to replace traditional temperature sensors because they can be operated in some harsh environments such as electrical power stations, coal mines, oil refineries. Furthermore, the FIR technique, which takes the advantage of temperature dependence of two thermally coupled energy levels of RE ions, is independent of spectral losses and fluctuations in the excitation intensity, resulting in high accuracy.<sup>11,12</sup>

The trivalent erbium ion (Er<sup>3+</sup>) is the most studied RE ion for this specific application, and Yb<sup>3+</sup> is usually employed as the co-doped ion to sensitize Er<sup>3+</sup>. Green UC luminescence of Er<sup>3+</sup> originate from two thermal coupled levels (<sup>2</sup>H<sub>11/2</sub> and <sup>4</sup>S<sub>3/2</sub>), whose emission intensity ratio would vary with environment temperature. It is well known that the Er<sup>3+</sup> <sup>2</sup>H<sub>11/2</sub> → <sup>4</sup>I<sub>15/2</sub> transition is

hypersensitive, and the temperature sensitivity of the materials varies remarkably for Er<sup>3+</sup> ions in different hosts.<sup>8–17</sup> Therefore, finding a host capable to provide suitable crystal field environment surrounding Er<sup>3+</sup> dopant to enhance radiative probability of the <sup>2</sup>H<sub>11/2</sub>–<sup>4</sup>I<sub>15/2</sub> hypersensitive transition is a key for obtaining high temperature sensitivity of Er<sup>3+</sup>.

NaGd(WO<sub>4</sub>)<sub>2</sub> is a member of the alkali rare earth tungstates (ARE(WO<sub>4</sub>)<sub>2</sub>, where A = alkali metal ions, RE = rare earth ions) family. It is considered to be a promising luminescent host lattice because of its good chemical durability and excellent physical properties as well as the relatively low lattice phonon energy. Recently, several chemical synthesis techniques to prepare RE doped NGW phosphors are available such as high temperature solid-state reaction,<sup>18</sup> sol-gel method,<sup>19</sup> hydrothermal method.<sup>20</sup> Hydrothermal method is better over other conventional techniques in terms of its better homogeneity, low cost, low processing temperature, less energy consumption and uniformity in particle size. It was reported that strong luminescence properties can be observed in RE (such as Pr<sup>3+</sup>, Sm<sup>3+</sup>, Eu<sup>3+</sup> and Dy<sup>3+</sup>) doped NGW phosphors.<sup>18–21</sup> However, to the best of our knowledge, there is little or no investigation on the UC emission and temperature sensing performances of NGW:Yb<sup>3+</sup>/Er<sup>3+</sup> microcrystals prepared by hydrothermal method. We report here the hydrothermal synthesis of the Yb<sup>3+</sup>/Er<sup>3+</sup> co-doped NGW microcrystals. The luminescence properties of NGW:Yb<sup>3+</sup>/Er<sup>3+</sup> microcrystals are investigated by changing doping concentrations of Yb<sup>3+</sup> (and Er<sup>3+</sup>) ions in the host. Additionally, their thermometry behaviors have also been illustrated by FIR technique.

School of Metallurgy and Chemical Engineering, Jiangxi University of Science and Technology, Center for Rare-earth Optoelectronic Materials, Ganzhou 341000, Jiangxi Province, P. R. China. E-mail: jsliao1209@126.com

## Experimental

### Sample preparation

All the chemicals of  $\text{Gd}_2\text{O}_3$  (99.99%),  $\text{Er}_2\text{O}_3$  (99.99%),  $\text{Yb}_2\text{O}_3$  (99.99%),  $\text{Na}_2\text{WO}_4 \cdot 2\text{H}_2\text{O}$  (AR), oleic acid (AR),  $\text{HNO}_3$  and  $\text{NaOH}$  were used as the starting materials without any further purification.  $\text{NGW:Yb}^{3+}/\text{Er}^{3+}$  samples for different  $\text{Yb}^{3+}$  doping concentration (12–24 at%) with a fixed  $\text{Er}^{3+}$  concentration (2 at%) and  $\text{Er}^{3+}$  doping concentration (1–10 at%) with a fixed  $\text{Yb}^{3+}$  concentration (20 at%) were prepared by oleic acid assisted hydrothermal method. A typical procedure for the  $\text{NGW:Yb}^{3+}/\text{Er}^{3+}$  (Yb 20 at%, Er 6 at%) sample synthesis as an example is described as follows: 0.1341 g  $\text{Gd}_2\text{O}_3$ , 0.0115 g  $\text{Er}_2\text{O}_3$  and 0.0397 g  $\text{Yb}_2\text{O}_3$  were first dissolved in dilute nitric acid under heating. After the  $\text{Gd}_2\text{O}_3$ ,  $\text{Er}_2\text{O}_3$  and  $\text{Yb}_2\text{O}_3$  were completely dissolved, the extra nitric acid was removed by evaporation. Then deionized water was added to obtain  $\text{Gd}(\text{NO}_3)_3$ ,  $\text{Er}(\text{NO}_3)_3$  and  $\text{Yb}(\text{NO}_3)_3$  mixed solution. Buffer solution of oleic acid and sodium oleate was obtained by mixture 0.5649 g pure oleic acid dissolved in 3 mL ethanol and 0.0400 g sodium hydroxide dissolved in 5 mL water. The buffer solution was added to the above mixed solution. Meanwhile 0.6597 g  $\text{Na}_2\text{WO}_4 \cdot 2\text{H}_2\text{O}$  was dissolved in deionized water while stirring. Second, the obtained  $\text{Na}_2\text{WO}_4$  solution was slowly added to the mixed solution with magnetic stirring to form white precipitate. The solution of white precipitate contained was transferred into a Teflon-lined stainless-steel autoclave, and heated to 200 °C for 24 h. Afterward the autoclave was cooled to room temperature naturally. Then the precipitate was collected and washed three times with absolute alcohol. After being dried in air at 80 °C for 8 h, the final powder products were obtained. To investigate the effect of  $\text{Yb}^{3+}$  and  $\text{Er}^{3+}$  content on the luminescence intensity, the other phosphor samples with different  $\text{Yb}^{3+}$  and  $\text{Er}^{3+}$ -codoped concentration were prepared by the same procedure with the corresponding starting materials.

### Characterization

X-ray diffractometer (XRD) patterns of samples were examined on a X'Pert PRO (PANalytical) powder diffractometer with  $\text{Cu-K}\alpha$  ( $\lambda = 0.150465$  nm) radiation to identify the crystal phase. The morphology of the samples was characterized by a JSM6700F scanning electron microscope (SEM) and a JEOL-2010 transmission electron microscope (TEM) equipped with the energy dispersive X-ray spectrum (EDS). In order to investigate the temperature dependence of the UC emission, the sample was placed in a temperature-controlled copper cylinder, and its temperature was increased from 293 to 573 K. The UC spectra of sample at various temperatures were obtained using a Fluorolog-3 double monochromator equipped with a Hamamatsu R928 Photomultiplier under the excitation of a 980 nm diode laser with 150 mW (the power density is about  $3 \text{ W cm}^{-2}$ ).

## Results and discussion

### Structure and morphology

The phase composition and purity of the  $\text{NGW:Yb}^{3+}/\text{Er}^{3+}$  product obtained by OA-assisted hydrothermal method were

examined by XRD technique. Fig. 1 shows XRD patterns of the  $\text{Yb}^{3+}/\text{Er}^{3+}$ -codoped NGW sample for (a) various  $\text{Yb}^{3+}$  concentrations up to 24 at% with a fixed 2 at%  $\text{Er}^{3+}$  and (b) various  $\text{Er}^{3+}$  concentrations up to 10 at% with a fixed 20 at%  $\text{Yb}^{3+}$ . The peak positions agree well with those of the standard diffraction pattern of NGW (JCPDS no. 25-829). The NGW compound belongs to tetragonal structure (scheelite  $\text{CaWO}_4$ ), which has the cell parameters of  $a = b = 0.5243$  nm,  $c = 1.1368$  nm, and  $Z = 4$ . There are two crystallographic positions of cations in the unit cell: 8-fold coordinated  $\text{Na}^+$  sites and 8-fold coordinated  $\text{Gd}^{3+}$  sites in the crystal structure of  $\text{NaGd}(\text{WO}_4)_2$ . According to the effective ionic radii of cations, the  $\text{Yb}^{3+}/\text{Er}^{3+}$  ions are proposed to occupy the  $\text{Gd}^{3+}$  sites or  $\text{Na}^+$  sites, because the effective radii of  $\text{Yb}^{3+}$  ions (0.0985 nm for CN = 8) and  $\text{Er}^{3+}$  ions (0.1004 nm for CN = 8) are highly close to those of both  $\text{Gd}^{3+}$  ions (0.1053 nm for CN = 8) and  $\text{Na}^+$  ions (0.118 nm for CN = 8). However, on the basis of the valence state analysis, the  $\text{Yb}^{3+}$  and  $\text{Er}^{3+}$  ions are much more probably occupying the  $\text{Gd}^{3+}$  sites. It is noted that the diffraction peak (112) of  $\text{NGW:Yb}^{3+}/\text{Er}^{3+}$  samples slightly shift to the high-angle. Because the radii of  $\text{Yb}^{3+}$  and  $\text{Er}^{3+}$  are slightly smaller than that of  $\text{Gd}^{3+}$ ,  $\text{Yb}^{3+}$  and  $\text{Er}^{3+}$  can be easily doped into host lattice and substituted for the site of  $\text{Gd}^{3+}$ .

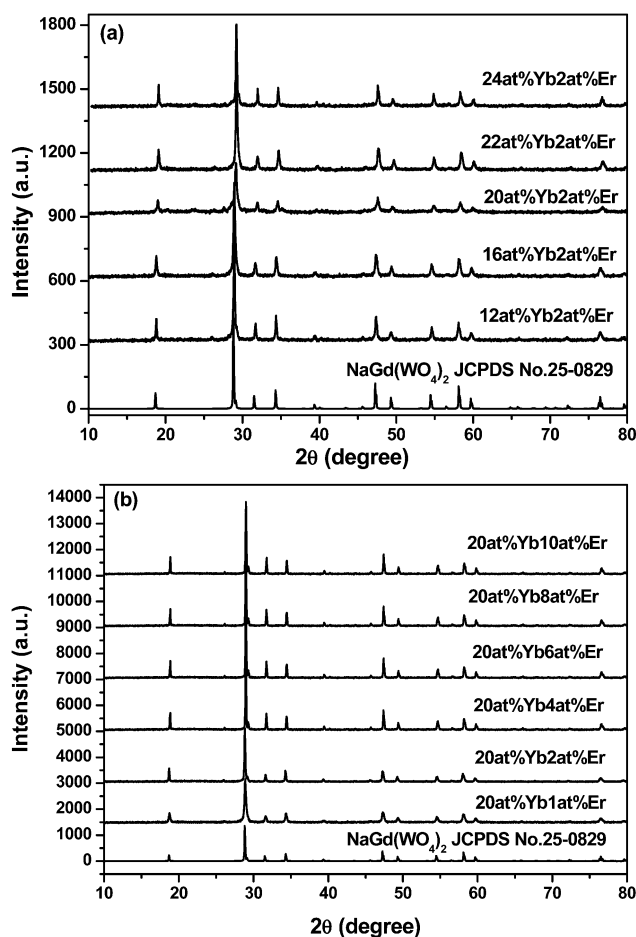


Fig. 1 XRD patterns for  $\text{NGW:Yb}^{3+}/\text{Er}^{3+}$  with (a)  $\text{Yb}^{3+}$  concentration from 12 to 24 at% with a fixed 2 at% Er and (b)  $\text{Er}^{3+}$  concentration from 1 to 10 at% with a fixed 20 at% Yb samples. The standard data for  $\text{NaGd}(\text{WO}_4)_2$  (JCPDS no. 25-829) is also presented in the figure.

ions. We conclude that  $\text{Yb}^{3+}$  and  $\text{Er}^{3+}$  have been efficiently incorporated into the host lattice of NGW crystal.

Fig. 2 shows SEM low- (a) and high- (b) magnification images of the  $\text{Yb}^{3+}/\text{Er}^{3+}$  co-doped NGW sample  $\text{Yb}^{3+}$  doped at 20 at% with  $\text{Er}^{3+}$  6 at%, which shows the morphology is nearly octahedra and the particle size is about 1.2  $\mu\text{m}$ . Morphological observation by transmission electron microscopy (TEM) is also shown in Fig. 2c. The TEM image of the  $\text{Yb}^{3+}/\text{Er}^{3+}$  co-doped NGW sample indicates the particle size is 1.2  $\mu\text{m}$ , which accords well with the result of SEM. The EDS was used to further characterize the chemical composition of the as-prepared product, and the results shown in Fig. 2f confirm that element ratios consist with the chemical formula of  $\text{Yb}^{3+}/\text{Er}^{3+}$  co-doped NGW sample for  $\text{Yb}^{3+}$  20 at% and  $\text{Er}^{3+}$  6 at%, with the  $\text{Yb} : \text{Er} : \text{Gd}$  molar ratio close to 10 : 3 : 37. The results confirm that  $\text{Yb}^{3+}$  and  $\text{Er}^{3+}$  ions have been effectively incorporated into the NGW host lattice, agreeing with the XRD analysis above.

Combining with the high resolution TEM image (HRTEM) (Fig. 2e), it can be clearly seen that the lattice fringes show the imaging characteristics in which the scheelite structure NGW crystal where the interplanar spacing of 0.3072 nm corresponds to the distance of the (112) planes. The selected area electron diffraction (SAED) pattern (Fig. 2d) from  $\text{NGW}:\text{Yb}^{3+}/\text{Er}^{3+}$  sample further clearly exhibited the single crystalline nature. The above results indicated that the  $\text{NaGd}(\text{WO}_4)_2:\text{Yb}^{3+}/\text{Er}^{3+}$  microcrystals can be successfully obtained by one-step hydrothermal method.

#### UC and NIR luminescence studies

In order to investigate concentration quenching of  $\text{Yb}^{3+}/\text{Er}^{3+}$  co-doped NGW, Fig. 3a and b shows the dependence of the UC luminescence spectra of the  $\text{Yb}^{3+}/\text{Er}^{3+}$  co-doped NGW phosphors on the sensitizer ( $\text{Yb}^{3+}$ ) and activator ( $\text{Er}^{3+}$ ) concentrations, respectively. Intense green emission at 532 and 554 nm ( $^2\text{H}_{11/2} \rightarrow ^4\text{I}_{15/2}$  and  $^4\text{S}_{3/2} \rightarrow ^4\text{I}_{15/2}$  transitions of  $\text{Er}^{3+}$ ) and very weak red

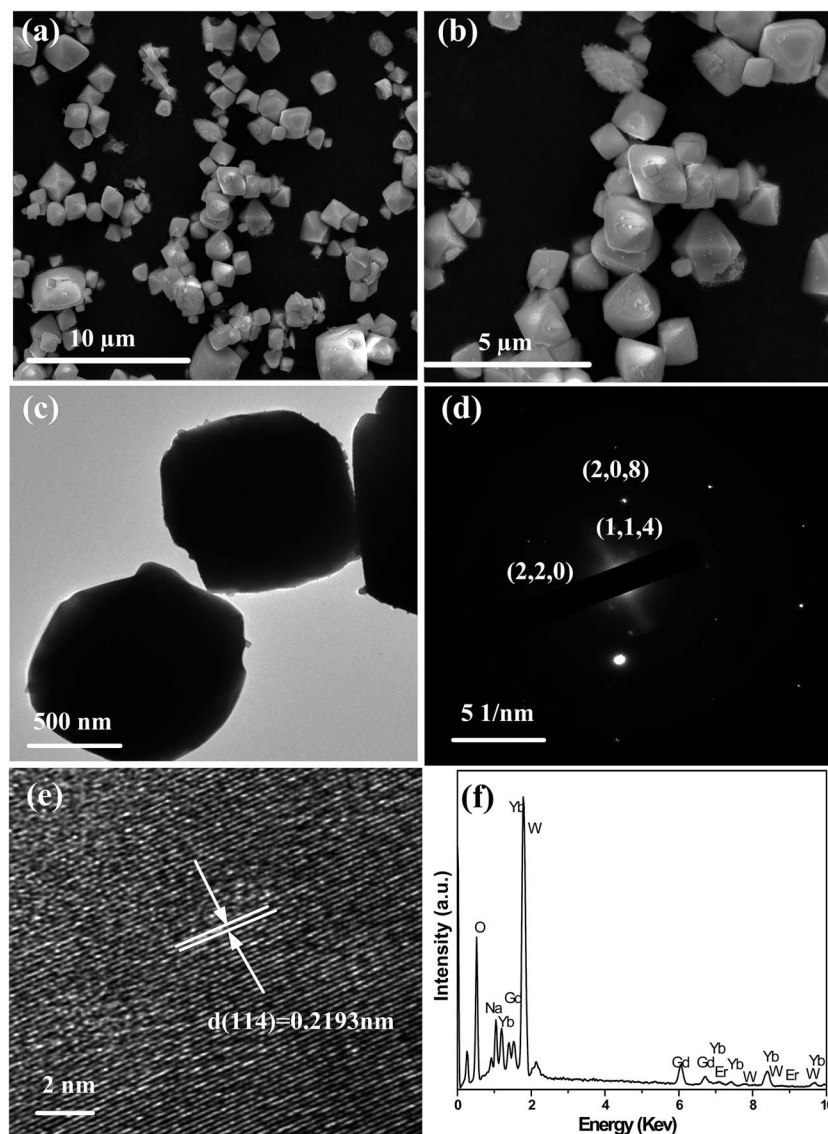


Fig. 2 Low- (a) and high-magnification (b) SEM image of the  $\text{NGW}:\text{Yb}^{3+}/\text{Er}^{3+}$  sample; (c) TEM image of  $\text{NGW}:\text{Yb}^{3+}/\text{Er}^{3+}$  sample; (d) EDS data taken from a single particle; (e) HRTEM image of  $\text{NGW}:\text{Yb}^{3+}/\text{Er}^{3+}$  sample; (f) SAED spectrum of  $\text{NGW}:\text{Yb}^{3+}/\text{Er}^{3+}$  sample.

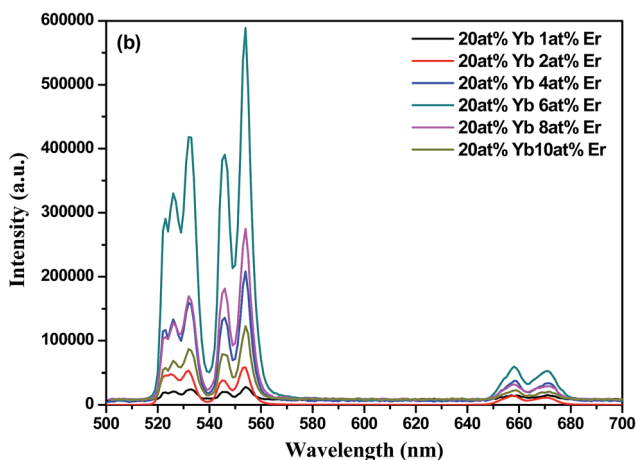
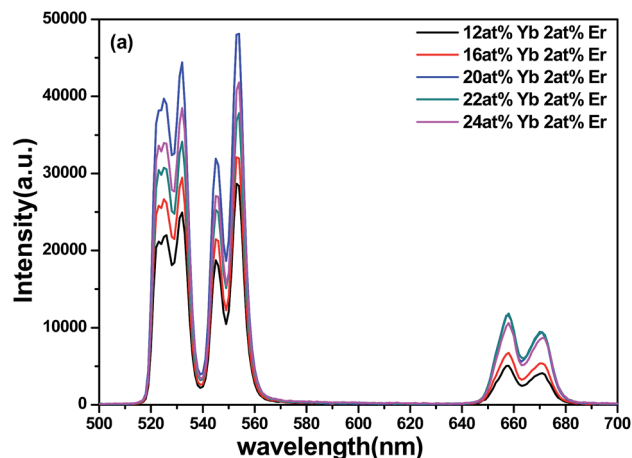


Fig. 3 UC emission spectra of the NGW:Yb<sup>3+</sup>/Er<sup>3+</sup> samples for (a) different Yb<sup>3+</sup> concentration with a fixed 2 at% Er and (b) different Er<sup>3+</sup> concentration a fixed 20 at% Yb under 980 nm excitation (the excitation power density is 3 W cm<sup>-2</sup>).

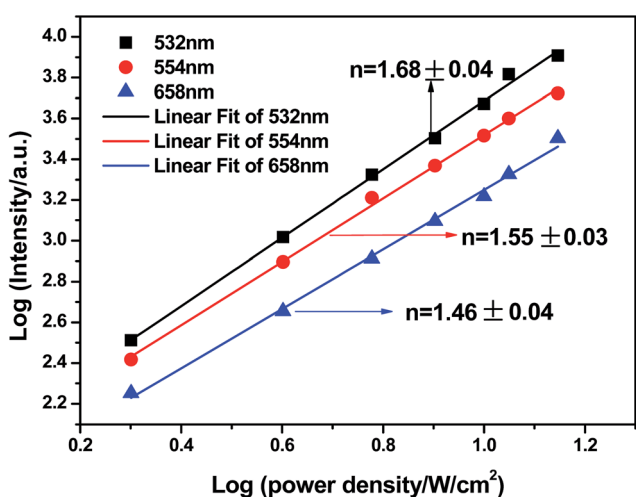


Fig. 4 Dependences of the UC intensities ( $I_{em}$ ) of  ${}^2H_{11/2}$ ,  ${}^4S_{3/2} \rightarrow {}^4I_{15/2}$  and  ${}^4F_{9/2} \rightarrow {}^4I_{15/2}$  transitions on the 980 nm pumping laser power ( $I_p$ ) for NGW:Yb<sup>3+</sup>/Er<sup>3+</sup> phosphors.

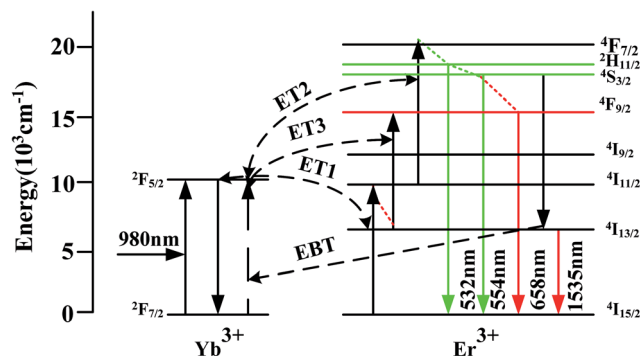


Fig. 5 Energy level diagrams of Yb<sup>3+</sup> and Er<sup>3+</sup> ions and UC emission mechanism in NGW:Yb<sup>3+</sup>/Er<sup>3+</sup> microcrystals.

emission at 658 nm ( ${}^4F_{9/2} \rightarrow {}^4I_{15/2}$  transition of Er<sup>3+</sup>) are observed in the emission spectra. As the concentrations of Er<sup>3+</sup> are fixed at 2 at%, the green emission intensity becomes stronger with the increasing of Yb<sup>3+</sup> content and reaches a maximum at 20 at% in the range of 12–24 at%, which is shown in Fig. 5a. The concentration quenching effect appears in this system and results in intensity decreasing as the concentration of Yb<sup>3+</sup> over 20 at%. This is believed to be due to the onset of the quenching effect that transfers the excitation of Er<sup>3+</sup> back to Yb<sup>3+</sup> and self-quenching in high-Yb<sup>3+</sup> doping concentration.<sup>22,23</sup> As the concentrations of Yb<sup>3+</sup> are fixed at 20 at%, the green emission intensity becomes stronger with the increasing of Er<sup>3+</sup> content and reaches a maximum at 6 at% in the range of 1–10 at% (see Fig. 5b). The concentration quenching effect is caused by the migration of excitation energy from one activator to another until a quenching site is reached and the energy is lost nonradiatively. The concentration quenching will not occur at low concentration, because the distance between identical Er<sup>3+</sup> ions is so large that the energy migration is hampered.<sup>24</sup> With the increase of the Er<sup>3+</sup> concentration, the average distance between Er<sup>3+</sup> ions become shorter and the energy transfer become convenient. The critical distance of which can prevent the energy transfer happening can be calculated by the following formula:<sup>25</sup>

$$R_c = 2(3V/4\pi NX_c)^{1/3}$$

where  $V$  is the volume of the unit cell,  $X_c$  is the critical concentration and  $N$  is the number of available crystallographic sites occupied by the activator ions in the unit cell. The values of  $V$  and  $N$  for the crystalline NGW (tetragonal system,  $a = b = 0.5243$  nm,  $c = 1.1368$  nm,  $Z = 4$ ,  $V = abc$ ,  $N = Z$ ) are 0.3125 nm<sup>3</sup> and 4, respectively. Considering the above optimum concentration as the critical concentration  $X_c$ , the  $R_c$  for Er<sup>3+</sup> is 1.355 nm in the NaGd<sub>0.74</sub>Yb<sub>0.2</sub>Er<sub>0.06</sub>(WO<sub>4</sub>)<sub>2</sub> phosphors.

To better understand the UC mechanism, the intensities of UC emissions were recorded as a function of the 980 nm excitation intensity in NGW:Yb<sup>3+</sup>/Er<sup>3+</sup> microcrystals (Fig. 4). The emission intensity  $I_{em}$  depends on the excitation power  $I_p$  following to the relationship of  $I_{em} \propto (I_p)^n$ , where  $n$  is the number of the pumping photons required to excite RE ions from the ground state to the emitting excited state. The power

dependence of the aforementioned three emission transitions is presented in Fig. 4 by a log-log plot. The slopes ( $n$ ) of the linear fittings are 1.68 for  ${}^2\text{H}_{11/2} \rightarrow {}^4\text{I}_{15/2}$ , 1.55 for  ${}^4\text{S}_{3/2} \rightarrow {}^4\text{I}_{15/2}$  and 1.46 for  ${}^4\text{F}_{9/2} \rightarrow {}^4\text{I}_{15/2}$ , indicating that two-photon processes are required to populate the  ${}^2\text{H}_{11/2}$ ,  ${}^4\text{S}_{3/2}$  and  ${}^4\text{F}_{9/2}$  emitting levels, respectively.

Fig. 5 illustrates the energy level diagrams with transitions which may be involved in the energy transfer process between  $\text{Yb}^{3+}$  and  $\text{Er}^{3+}$  in  $\text{NGW}:\text{Yb}^{3+}/\text{Er}^{3+}$  microcrystals. As for  $\text{Yb}^{3+}/\text{Er}^{3+}$  codoped system under 980 nm excitation, the 980 nm laser photon excites the  $\text{Yb}^{3+}$  ion from the  ${}^2\text{F}_{7/2}$  ground state to the  ${}^2\text{F}_{5/2}$  excited state. And the excited  $\text{Yb}^{3+}$  ion in the  ${}^2\text{F}_{5/2}$  state transfers its excitation energy to one nearby  $\text{Er}^{3+}$  ion. The  $\text{Er}^{3+}$  ion at the ground  ${}^4\text{I}_{15/2}$  state is excited to the upper  ${}^4\text{F}_{7/2}$  state *via* two energy transfer (ET<sub>1</sub> and ET<sub>2</sub>) processes.<sup>26</sup> Subsequently, the non-radiative relaxation process of  ${}^4\text{F}_{7/2}$  state populates two lower energy levels ( ${}^2\text{H}_{11/2}$  and  ${}^4\text{S}_{3/2}$ ), resulting in the green ( ${}^2\text{H}_{11/2} \rightarrow {}^4\text{I}_{15/2}$  and  ${}^4\text{S}_{3/2} \rightarrow {}^4\text{I}_{15/2}$ ) UC emissions. The weak red UC emission centered at 658 nm is originated from  ${}^4\text{F}_{9/2} \rightarrow {}^4\text{I}_{15/2}$  transition. There exist two main possible pumping mechanisms for red emission (detailed discussion description see ref. 10).

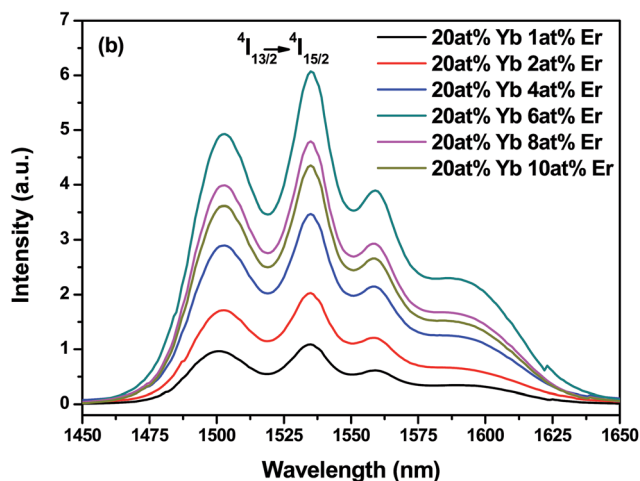
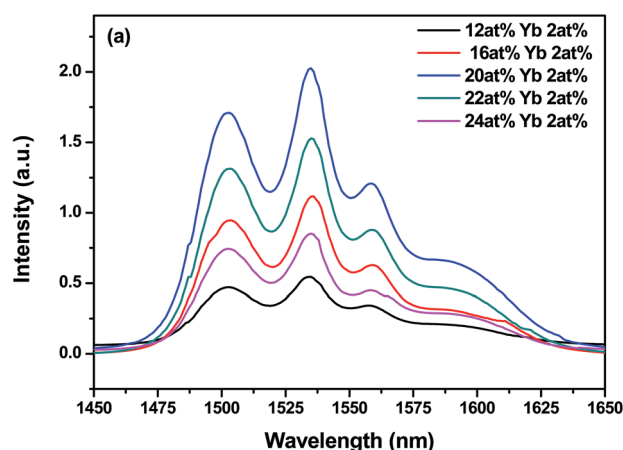


Fig. 6 NIR emission spectra of the  $\text{NGW}:\text{Yb}^{3+}/\text{Er}^{3+}$  samples for (a) different  $\text{Yb}^{3+}$  concentration with a fixed 2 at%  $\text{Er}^{3+}$  and (b) different  $\text{Er}^{3+}$  concentration with a fixed 20 at%  $\text{Yb}^{3+}$  under 980 nm excitation (the excitation power density is  $3 \text{ W cm}^{-2}$ ).

Fig. 6 shows a broad NIR luminescence spectra of the  $\text{NGW}:\text{Yb}^{3+}/\text{Er}^{3+}$  microcrystals for different  $\text{Yb}^{3+}$  ( $\text{Er}^{3+}$ ) doping concentrations under 980 nm excitation. As can be seen from the energy level diagrams (Fig. 5), the NIR emission centered at 1535 nm is due to the transition of  $\text{Er}^{3+}:$  ${}^4\text{I}_{13/2} \rightarrow {}^4\text{I}_{15/2}$ . Similar to relationship between the UC emission intensity and  $\text{Yb}^{3+}$  ( $\text{Er}^{3+}$ ) doping concentrations, the luminescence intensity increase obviously with the increase of  $\text{Yb}^{3+}$  ( $\text{Er}^{3+}$ ) doping concentrations at a certain range of  $\text{Yb}^{3+}$  ( $\text{Er}^{3+}$ ) doping concentrations. Significantly, the 1535 nm luminescence intensity also increases with the increase of  $\text{Yb}^{3+}$  ( $\text{Er}^{3+}$ ) doping concentration and reaches the maximum at 20 at% (6 at%), and then decreases with the increase of  $\text{Yb}^{3+}$  ( $\text{Er}^{3+}$ ) doping concentration.

### Effect of temperature on UC emission and temperature-sensing behaviour

As already mentioned, UC bands centered at 532 and 554 nm arise from  ${}^2\text{H}_{11/2} \rightarrow {}^4\text{I}_{15/2}$  and  ${}^4\text{S}_{3/2} \rightarrow {}^4\text{I}_{15/2}$  transitions. The energy gap between the levels  ${}^2\text{H}_{11/2}$  and  ${}^4\text{S}_{3/2}$  of  $\text{Er}^{3+}$  is around  $747 \text{ cm}^{-1}$ , the state of  ${}^2\text{H}_{11/2}$  may also be populated from  ${}^4\text{S}_{3/2}$  by thermal excitation and the UC emission intensity ratio of emission band at 532 to 554 nm could change with the variable temperature, therefore it is could be used as optically temperature sensor for the present UC phosphors. In order to investigate the temperature sensing properties of synthesized phosphors, the green UC emission spectra for  $\text{NGW}:20 \text{ at% } \text{Yb}^{3+}/6 \text{ at% } \text{Er}^{3+}$  phosphor at different temperature (from 293 to 523 K) are shown in Fig. 7, in which the spectra are normalized to the emission peak at 554 nm. In present cases, the excitation power density was estimated to be around  $3 \text{ W cm}^{-2}$ , which is low enough to neglect the heating effect from the pumping source. It is found that no remarkable shift in emission wavelength for the sample while the fluorescence intensity ratio (FIR) of UC emission from  ${}^2\text{H}_{11/2} \rightarrow {}^4\text{I}_{15/2}$  to  ${}^4\text{S}_{3/2} \rightarrow {}^4\text{I}_{15/2}$  increases with the rise of temperature. The relative population of the thermally coupled energy levels follows the Boltzmann distribution and the FIR of two emissions can be written as follows:<sup>27</sup>

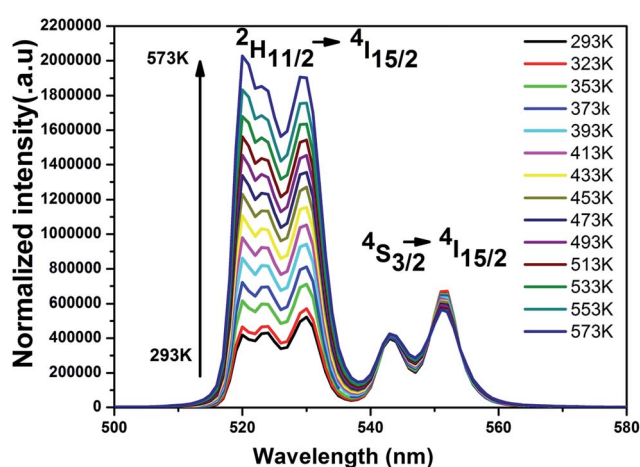


Fig. 7 Temperature dependence of the green UC luminescence spectra of  $\text{NGW}:\text{Yb}^{3+}/\text{Er}^{3+}$  phosphor under 980 nm excitation (the spectra are normalized to the emission peak at 554 nm. The excitation power density is  $3 \text{ W cm}^{-2}$ ).

$$\text{FIR} = \frac{I_H}{I_S} = \frac{n_H}{n_S} = \frac{g_H \omega_H \delta_H}{g_S \omega_S \delta_S} \exp\left(\frac{-\Delta E}{kT}\right) = B \exp\left(\frac{-\Delta E}{kT}\right) \quad (1)$$

where  $I_H$  and  $I_S$  are intensities (the integrated areas below the emission curves) for the upper ( ${}^2\text{H}_{11/2} \rightarrow {}^4\text{I}_{15/2}$ ) and lower ( ${}^4\text{S}_{3/2} \rightarrow {}^4\text{I}_{15/2}$ ) thermally coupled levels transitions,

respectively. In general,  $N$ ,  $g$ ,  $\omega$ ,  $\delta$  represent the number of ions, the degeneracy, the angular frequency, the emission cross section of fluorescence transitions from excited state ( ${}^2\text{H}_{11/2}$  and  ${}^4\text{S}_{3/2}$ ) to the ground state ( ${}^4\text{I}_{15/2}$ ), respectively.  $\Delta E$  is the energy gap between the  ${}^2\text{H}_{11/2}$  and  ${}^4\text{S}_{3/2}$  levels,  $k$  is the Boltzmann constant, and  $T$  is the absolute temperature.  $B$  is the pre-exponential factor.

The fluorescent intensity ratio (FIR) of these two UC emissions shows a remarkable dependence on the temperature (Fig. 8a). According to the expression of the FIR, the value of  $\ln(\text{FIR})$  versus the inverse absolute temperature ( $1/T$ ) is plotted in Fig. 8b. The linear fitting of the experimental data gave slope and intercept equal to  $895.54 \pm 29.00$  and  $2.95 \pm 0.07$ , respectively. As a consequence, the energy gap  $\Delta E$  and the pre-exponential constant are evaluated to be about  $621 \text{ cm}^{-1}$  and  $19.11$ , respectively. These two parameters are vital factors for the sensitivity ( $S$ ) of temperature detection, as defined by the following equation<sup>27</sup>

$$S = \frac{d\text{FIR}}{dT} = \text{FIR} \left( \frac{\Delta E}{kT^2} \right) = B \left( \frac{\Delta E}{kT^2} \right) \exp\left(-\frac{\Delta E}{kT}\right) \quad (2)$$

where the term FIR is the symbol used for fluorescence intensity ratio. The calculated values of sensor sensitivity were plotted as a function of absolute temperature (see Fig. 8c) and found to be maximum about  $114.96 \times 10^{-4} \text{ K}^{-1}$  at 453 K. As a comparison, the optical thermometry parameters in some typical  $\text{Er}^{3+}/\text{Yb}^{3+}$  co-doped UC materials are tabulated in Table 1. From Table 1, the temperature sensitivity of  $\text{NGW}:\text{Yb}^{3+}/\text{Er}^{3+}$  phosphor is higher than those of  $\text{La}_2\text{O}_3:\text{Yb}^{3+}/\text{Er}^{3+}$ ,  $\text{La}_2\text{O}_2\text{S}:\text{Yb}^{3+}/\text{Er}^{3+}$ ,  $\text{Y}_2\text{Ti}_2\text{O}_7:\text{Yb}^{3+}/\text{Er}^{3+}$  and  $\text{NaY}(\text{MoO}_4)_2:\text{Yb}^{3+}/\text{Er}^{3+}$  phosphors, but slightly lower than that of  $\text{SrWO}_4:\text{Yb}^{3+}/\text{Er}^{3+}$  phosphor with the same scheelite structure (NGW). Therefore, the  $\text{Yb}^{3+}/\text{Er}^{3+}$  co-doped NGW phosphors can be used as an efficient optical temperature sensor.

To better investigate the effect of temperature on the luminescence dynamics of  $\text{Er}^{3+}$  ions for the thermally coupled  ${}^2\text{H}_{11/2}$  and  ${}^4\text{S}_{3/2}$  states, we measured the luminescence decay curves of two green UC emission bands ( ${}^2\text{H}_{11/2}$  and  ${}^4\text{S}_{3/2}$  states) of  $\text{Er}^{3+}$  ions at different temperatures (293, 393, 453 K). As shown in Fig. 9, the luminescence decay curves of  $\text{Er}^{3+}$  ions for the thermally coupled  ${}^2\text{H}_{11/2}$  and  ${}^4\text{S}_{3/2}$  states exhibit single-exponential decays at different temperatures. The lifetimes for  ${}^2\text{H}_{11/2}$  energy level of the  $\text{Er}^{3+}$  ions at 293, 393 and 453 K are about 10.98, 10.04, 9.75  $\mu\text{s}$ , respectively. The lifetimes for  ${}^4\text{S}_{3/2}$  energy level of the  $\text{Er}^{3+}$  ions at 293, 393 and 453 K are about 11.38, 10.36, 9.83  $\mu\text{s}$ , respectively. This result shows that the luminescence lifetimes of the thermally coupled  ${}^2\text{H}_{11/2}$  and  ${}^4\text{S}_{3/2}$  for  $\text{NGW}:\text{Yb}^{3+}/\text{Er}^{3+}$  microcrystal slightly decrease as the temperature increases. Generally, the trend of temperature dependence of the quantum efficiency follows similarly that of the luminescence lifetime.<sup>28</sup> Thus we speculate that the quantum efficiency of the  $\text{NGW}:\text{Yb}^{3+}/\text{Er}^{3+}$  microcrystal has no obvious change with the increasing temperature. This would mean that the  $\text{NGW}:\text{Yb}^{3+}/\text{Er}^{3+}$  microcrystal maintains relatively high luminescence intensity at high temperature. As we know, the  $\beta\text{-NaYF}_4:\text{Yb}^{3+}/\text{Er}^{3+}$  phosphor is considered to be the most efficient UC emission material for green and red UC emission. The

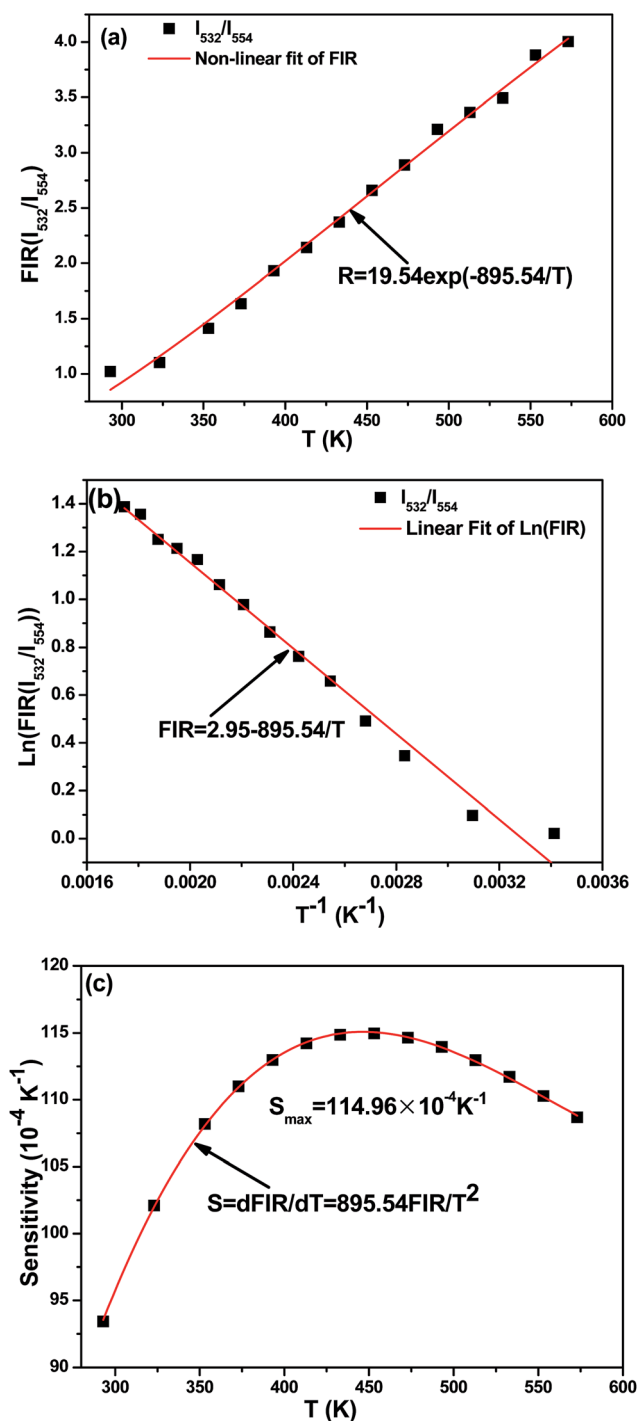


Fig. 8 Upconversion-based temperature-sensing behaviour of  $\text{NGW}:\text{Yb}^{3+}/\text{Er}^{3+}$  phosphor: (a) FIR relative to the temperature; (b) monolog plot of the FIR as a function of the inverse absolute temperature; (c) sensor sensitivity as a function of temperature.

Table 1 Optical thermometry parameters in some typical Yb<sup>3+</sup>/Er<sup>3+</sup> codoped UC materials temperature sensitivities with their temperature range

Sample	Temperature range (K)	Maximum sensitivity (K <sup>-1</sup> )	T <sub>max</sub> (K)	Reference
La <sub>2</sub> O <sub>3</sub> :Yb <sup>3+</sup> /Er <sup>3+</sup>	303–600	91 × 10 <sup>-4</sup>	303	9
La <sub>2</sub> O <sub>2</sub> S:Yb <sup>3+</sup> /Er <sup>3+</sup>	200–600	80 × 10 <sup>-4</sup>	562	13
Y <sub>2</sub> Ti <sub>2</sub> O <sub>7</sub> :Yb <sup>3+</sup> /Er <sup>3+</sup>	298–673	67.32 × 10 <sup>-4</sup>	363	14
NaY(MoO <sub>4</sub> ) <sub>2</sub> :Yb <sup>3+</sup> /Er <sup>3+</sup>	303–523	97 × 10 <sup>-4</sup>	493	15
SrWO <sub>4</sub> :Yb <sup>3+</sup> /Er <sup>3+</sup>	300–420	149.8 × 10 <sup>-4</sup>	403	16
β-NaYF <sub>4</sub> :Yb <sup>3+</sup> /Er <sup>3+</sup>	75–600	48.4 × 10 <sup>-4</sup>	515	17
NaY(WO <sub>4</sub> ) <sub>2</sub> :Yb <sup>3+</sup> /Er <sup>3+</sup>	133–773	112 × 10 <sup>-4</sup>	515	10
NaGd(WO <sub>4</sub> ) <sub>2</sub> :Yb <sup>3+</sup> /Er <sup>3+</sup>	293–573	114.96 × 10 <sup>-4</sup>	453	This work

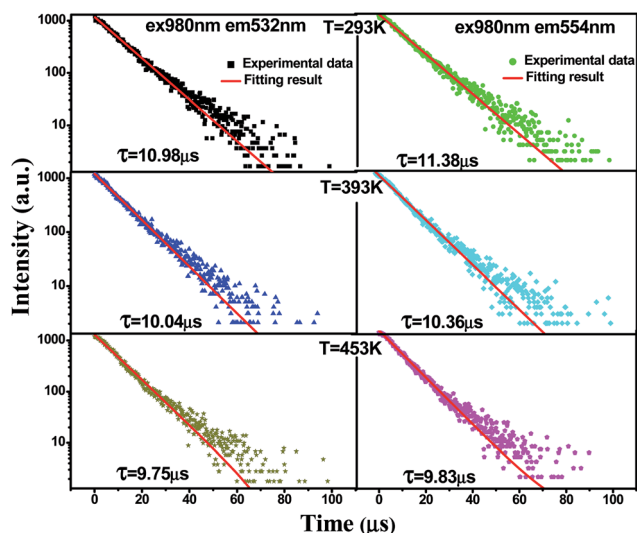


Fig. 9 Luminescence decay curves of Er<sup>3+</sup> ions for the thermally coupled <sup>2</sup>H<sub>11/2</sub> (532 nm left) and <sup>4</sup>S<sub>3/2</sub> (554 nm right) states in NGW:20 at% Yb<sup>3+</sup>/6 at% Er<sup>3+</sup> microcrystal at different temperatures.

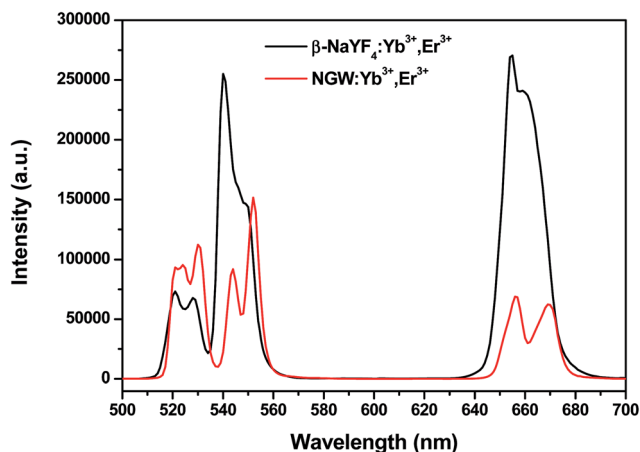


Fig. 10 The UC emission spectra of the NGW:Yb<sup>3+</sup>/Er<sup>3+</sup> microcrystal and β-NaYF<sub>4</sub>:Yb<sup>3+</sup>/Er<sup>3+</sup> at room temperature (excitation wavelength 980 nm, excitation power density 3 W cm<sup>-2</sup>).

comparison of the luminescence spectra of the NGW:Yb<sup>3+</sup>/Er<sup>3+</sup> and β-NaYF<sub>4</sub>:Yb<sup>3+</sup>/Er<sup>3+</sup> under the excitation wavelength of 980 nm are shown in Fig. 10. The integrate emission intensity of NGW:Yb<sup>3+</sup>/Er<sup>3+</sup> microcrystal is about half as strong as that of β-NaYF<sub>4</sub>:Yb<sup>3+</sup>/Er<sup>3+</sup>, nevertheless, the maximum sensitivity of NGW:Yb<sup>3+</sup>/Er<sup>3+</sup> microcrystal is about 2.4 times as much as that of β-NaYF<sub>4</sub>:Yb<sup>3+</sup>/Er<sup>3+</sup> (see Table 1).<sup>17</sup> Therefore, NGW:Yb<sup>3+</sup>/Er<sup>3+</sup> microcrystal is very promising materials for the application in optical thermometry.

## Conclusions

In summary, the NGW:Yb<sup>3+</sup>/Er<sup>3+</sup> microcrystals have been prepared by hydrothermal method. The intense visible UC and NIR luminescence of samples are clearly observed under 980 nm excitation. The mechanisms of UC and NIR luminescence and the changes of the emission intensity with Yb<sup>3+</sup> concentration or Er<sup>3+</sup> concentration are discussed. The transition mechanisms of the UC luminescence can be ascribed to a two-photon absorption process. The best doping concentration of NGW for UC and NIR emission is about 20 at% Yb<sup>3+</sup> and 6 at% Er<sup>3+</sup>. The green UC emission bands observed around 532 (<sup>2</sup>H<sub>11/2</sub> → <sup>4</sup>I<sub>15/2</sub>) and 554 nm (<sup>4</sup>S<sub>3/2</sub> → <sup>4</sup>I<sub>15/2</sub>) have been utilized for optical thermometry *via* the fluorescence intensity ratio technique. The dependence of FIR for the sample NGW:20 at% Yb<sup>3+</sup>/6 at% Er<sup>3+</sup> with optimal composition on temperature were measured in the range of 293–573 K, and the sensitivities of sample reach the maximum 114.96 × 10<sup>-4</sup> K<sup>-1</sup> at 453 K. All these results suggest that Yb<sup>3+</sup>/Er<sup>3+</sup> co-doped NGW phosphor materials can be explored UC fluorescence imaging and temperature measurements with high sensitivity.

## Acknowledgements

This work was financially supported by the National Natural Science Foundation of China (No. 51162012) and Natural Science Foundation of Jiangxi Province (No. 20142BAB203004).

## Notes and references

- 1 E. Downing, L. Hesselink, J. Ralston and R. Macfarlane, *Science*, 1996, **273**, 1185–1189.

- 2 T. J. Whitley, C. A. Millar, R. Wyatt, M. C. Brierley and D. Szebesta, *Electron. Lett.*, 1991, **27**, 1785–1786.
- 3 L. Li, C. F. Guo, S. Jiang, D. K. Agrawal and T. Li, *RSC Adv.*, 2014, **4**, 6391–6396.
- 4 J. De Wild, J. K. Rath, A. Meijerink, W. G. Van Sark and R. E. Schropp, *Sol. Energy Mater. Sol. Cells*, 2010, **94**, 2395–2398.
- 5 C. Zhang, H. P. Zhou, L. Y. Liao, W. Feng, W. Sun, Z. X. Li, C. H. Xu, C. J. Fang, L. D. Sun, Y. W. Zhang and C. H. Yan, *Adv. Mater.*, 2010, **22**, 633–637.
- 6 J. Pichaandi, J. C. Boyer, K. R. Delaney and F. C. J. M. van Veggel, *J. Phys. Chem. C*, 2011, **115**, 19054–19064.
- 7 L. Shang, S. Dong and G. U. Nienhaus, *Nano Today*, 2011, **6**, 401–418.
- 8 B. S. Cao, Y. Y. He, Z. Liu, Z. P. Li and B. Dong, *Sens. Actuators, B*, 2011, **159**, 8–11.
- 9 D. Riya and K. R. Vineet, *Dalton Trans.*, 2014, **43**, 111–118.
- 10 P. Du, L. H. Luo and J. S. Yu, *Ceram. Int.*, 2016, **42**, 5635–5641.
- 11 Y. Tian, B. Tian, C. Cui, P. Huang, L. Wang and B. Chen, *RSC Adv.*, 2015, **5**, 14123–14128.
- 12 D. He, C. Guo, S. Jiang, N. Zhang, C. Duan, M. Yin and T. Li, *RSC Adv.*, 2015, **5**, 1385–1390.
- 13 Y. M. Yang, C. Mi, F. Yu, X. Y. Su, C. F. Guo, G. Li, J. Zhang, L. L. Liu, Y. Z. Liu and X. D. Li, *Ceram. Int.*, 2014, **40**, 9875–9880.
- 14 B. P. Singh, A. K. Parchur, R. S. Ningthoujam, P. V. Ramakrishna, S. Singh, P. Singh, S. B. Rai and R. Maalej, *Phys. Chem. Chem. Phys.*, 2014, **6**(41), 22665–22676.
- 15 X. X. Yang, Z. L. Fu, Y. M. Yang, C. P. Zhang, Z. J. Wu and T. Q. Sheng, *J. Am. Ceram. Soc.*, 2015, **98**(8), 2595–2600.
- 16 A. Pandey, V. K. Rai, V. Kumar, V. Kumar and H. C. Swart, *Sens. Actuators, B*, 2015, **209**, 352–358.
- 17 L. I. Tong, X. P. Li, R. N. Hua, X. J. Li, H. Zheng, J. S. Sun, J. S. Zhang, L. H. Cheng and B. J. Chen, *J. Lumin.*, 2015, **167**, 386–396.
- 18 J. Chen, X. H. Gong, Y. F. Lin, Y. J. Chen, Z. D. Luo and Y. D. Huang, *J. Alloys Compd.*, 2010, **492**, 667–670.
- 19 A. Durairajan, D. Balaji, K. Kavi Rasu, S. Moorthy Babu, M. A. Valente, D. Thangaraju and Y. Hayakawa, *J. Lumin.*, 2016, **170**, 743–748.
- 20 J. S. Liao, H. Y. You, B. Qiu, H. R. Wen, R. J. Hong, W. X. You and Z. P. Xie, *Curr. Appl. Phys.*, 2011, **11**, 503–507.
- 21 Y. Liu, G. X. Lin, J. X. Wang, X. T. Dong and W. S. Yu, *Inorg. Chem.*, 2014, **53**, 11457–11466.
- 22 S. Hinojosa, M. A. Meneses-Nava, O. Barbosa-Garcia, L. A. Diaz-Torres, M. A. Santoyo and J. F. Mosino, *J. Lumin.*, 2003, **102–103**, 694–698.
- 23 F. Auzel, G. Baldacchini, L. Laversenne and G. Boulon, *Opt. Mater.*, 2003, **24**, 103–109.
- 24 C. F. Guo, X. Ding, H. J. Seoc, Z. Y. Rena and J. T. Bai, *J. Alloys Compd.*, 2011, **509**, 4871–4874.
- 25 G. Blasse, *Philips Res. Rep.*, 1969, **24**, 131–136.
- 26 J. H. Kim, H. Choi, E. O. Kim, H. M. Noh, B. K. Mon and J. H. Teong, *Opt. Mater.*, 2014, **38**, 113–118.
- 27 B. Dong, B. S. Cao and Y. Y. He, *Adv. Mater.*, 2012, **24**, 1987–1993.
- 28 X. Y. Chen, E. Ma, G. K. Liu and M. Yin, *J. Phys. Chem. C*, 2007, **111**, 9638–9643.